Earth Planets Space, **61**, 471–478, 2009

Gravity waves in the equatorial thermosphere and their relation to lower atmospheric variability

Yasunobu Miyoshi[1] and Hitoshi Fujiwara[2]

[1]*Department of Earth and Planetary Sciences, Faculty of Sciences, Kyushu University, 6-10-1, Hakozaki, Fukuoka, Japan*
[2]*Department of Geophysics, Faculty of Science, Tohoku University, Sendai, Japan*

(Received September 27, 2007; Revised June 23, 2008; Accepted June 24, 2008; Online published May 14, 2009)

Using a general circulation model that contains the region from the ground surface to the upper thermosphere, we have examined characteristics of gravity waves in the equatorial thermosphere. At an altitude of 150 km, the dominant periods of gravity waves for zonal wave number 20 (zonal wavelength $\lambda_x \approx 2000$ km), 40 ($\lambda_x \approx 1000$ km) and 80 ($\lambda_x \approx 500$ km) are 3, 1.5 and 1 h, respectively. For individual zonal wave numbers, the corresponding dominant period becomes shorter at higher altitudes due to dissipation processes in the thermosphere, such as molecular viscosity and ion drag force, indicating that gravity waves with a larger horizontal phase velocity (larger vertical wavelength) can penetrate into the thermosphere. The longitudinal variation of gravity wave activity in the equatorial thermosphere and upward propagation of gravity waves from the lower atmosphere were also studied. The longitudinal distribution of gravity wave activity in the thermosphere is quite similar to that of gravity wave activity in the lower atmosphere and the cumulus convective activity in the tropical troposphere. Our results indicate that the strong energy flux due to gravity waves from the enhanced cumulus convective activity propagates upward into the upper thermosphere. The relation between the wind fluctuation associated with gravity waves and the ionospheric variation is discussed. Fluctuations of the neutral zonal wind with periods of 1–2 h are significant in the 200- to 300-km height region, and its amplitude sometimes exceeds 50 m s^{-1}. These results suggest that upward propagating gravity waves can affect the ionospheric variation in the F-region.

Key words: Gravity waves, equatorial thermosphere, upward propagation, wind fluctuation, ionospheric variation.

1. Introduction

Gravity waves play an important role in the general circulation of the atmosphere in the stratosphere and mesosphere. Matsuno (1982) and Lindzen (1981) showed that the closing of mesospheric jets and the reversal of the zonal wind direction in the mesopause region were maintained by the gravity wave drag. Radar observations have revealed the behavior of gravity waves in the mesosphere and lower thermosphere (MLT). The vertical flux of zonal momentum due to gravity waves ($u'w'$) (u', w' denote the zonal and vertical wind fluctuation components, respectively) was found to be 1–5 m^2 s^{-2} at a height of 80–90 km over the middle latitudes and that $u'w'$ was eastward (westward) in summer (winter) (Reid and Vincent, 1987; Vincent and Fritts, 1987; Tsuda *et al*., 1990).

Using the GFDL SKYHI general circulation models (GCMs) with horizontal resolutions of N90 (a grid spacing of 1.0° latitude × 1.2° longitude) and N150 (0.6° × 0.72°), Hayashi *et al*. (1989, 1997) and Jones *et al*. (1997) investigated the characteristics of gravity waves in the stratosphere and mesosphere and the global distribution of $\overline{u'w'}$ ($\overline{\ }$ denotes the zonal mean) due to gravity waves. Sato *et al*. (1999) investigated the global distribution and characteristics of small vertical-scale gravity waves in the troposphere and lower stratosphere using a GCM with high resolution in both the horizontal and vertical directions. Thus, GCMs are quite useful tools for investigating characteristics of gravity waves and their momentum fluxes. However, the numerical studies carried out to date using a GCM have focused on gravity waves in the height range from the troposphere to the mesopause region. Using a GCM that contains the region from the ground surface to the upper thermosphere, Miyoshi and Fujiwara (2008; hereafter MF08) recently investigated the characteristics of gravity waves in the thermosphere and upward propagation of gravity waves from the lower atmosphere to the thermosphere. MF08 showed that upward propagating gravity waves played an important role in the general circulation of the thermosphere.

Due to an insufficient number of global observations of the wind, the behavior of gravity waves is not well known in the thermosphere. In fact, gravity waves in the thermosphere are observed indirectly as fluctuations of the ionospheric plasma (traveling ionospheric disturbance, TID). The horizontal scale of the observed TIDs ranges from several hundred kilometers to several thousand kilometers. Most of TIDs at high latitudes are considered to be generated by Joule heating, Lorentz force and/or auroral particle precipitation. In contrast, Waldock and Jones (1987) ray-traced most of the gravity waves back into the ground level

and showed a weak positive correlation between these gravity waves and tropospheric jet speed. Simultaneous wind measurements that cover the region from the troposphere to the thermosphere are impossible, thereby limiting the amount of knowledge available on the upward propagation of gravity waves from the troposphere to the thermosphere. Vadas and Fritts (2004, 2006) and Horinouchi *et al*. (2002) investigated the upward propagation of gravity waves generated by cumulus convection into the thermosphere using a regional model. Vadas (2007) recently reported the results of her investigation of the dissipative filtering of upward propagating gravity waves with 10- to 2000-km horizontal wavelengths. However, to date, there have only been a few theoretical studies on the upward propagation of gravity waves into the thermosphere.

Using GPS/MET (meteorology) radio occultation, Hocke and Tsuda (2001) investigated the longitudinal distributions of gravity wave activity in the stratosphere and E-region plasma irregularities (80- to 120-km heights). The E-region plasma irregularities are probably generated by atmospheric waves of the neutral atmosphere through the ion-neutral coupling process. As such, they clearly demonstrated that the longitudinal distribution of plasma irregularities in the MLT region was similar to that of the water vapor pressure in the tropics, indicating the dynamical coupling between the troposphere and the MLT region through the upward propagation of gravity waves. However, the longitudinal distribution of gravity wave activity above the MLT region and its relation to plasma irregularities in the F-region are not known. Therefore, in our study, we used a GCM that contains the region from the ground surface to the upper thermosphere to investigate the behavior of gravity waves in the equatorial thermosphere and the upward propagation of gravity waves from the lower atmosphere to the upper thermosphere. We focused our attention on the longitudinal variation in gravity wave activity in the equatorial thermosphere and its relation with the cumulus convection in the tropical troposphere. As mentioned above, fluctuations of the wind due to gravity waves in the thermosphere influence the variability of the ionospheric parameters (e.g., Hocke and Schlegel, 1996). Here, we discuss the wind fluctuation associated with gravity waves in the thermosphere and its relation to ionospheric variability. The descriptions of the GCM used in this study and the numerical simulation are presented in Section 2. The results and discussion are presented in Sections 3 and 4, respectively. A summary follows in Section 5.

2. Descriptions of the GCM and Numerical Simulations

The GCM used in this study is an extension of the middle atmosphere GCM developed at Kyushu University (Miyahara *et al*., 1993; Miyoshi, 1999). The model is the same as the GCM used by MF08. The horizontal resolution is T85 (maximum horizontal wave number = 85), which corresponds to a grid spacing of 1.4° latitude × 1.4° longitude, and the vertical resolution is 0.4 scale height above the tropopause. The GCM has 75 vertical levels and contains the region from the ground surface to the upper thermosphere. It solves the full nonlinear equations of eastward momentum, northward momentum and thermodynamics. The vertical velocity (ω) at a constant pressure level is calculated by solving the continuity equation, and the vertical wind velocity (w) is estimated from the vertical velocity (ω) at a constant pressure level. The GCM has a full set of the physical processes appropriate for investigating the troposphere, stratosphere, mesosphere and thermosphere (Miyoshi, 2006; Miyoshi and Fujiwara, 2006). A more detailed description of these physical processes is found in Miyoshi and Fujiwara (2003).

The GCM includes schemes for hydrology, a boundary layer, radiation, eddy diffusion and moist convection. The distributions of water vapor and cloud are predicted in the GCM, and the cumulus parameterization by Kuo is used. Effects of the surface topography and land-sea contrast are also taken into account. The monthly mean of zonally symmetric distribution of O_3 is prescribed. The gravity wave parameterization developed by McFarlane (1987) is used for orographic gravity waves, while the parameterization for non-orographic gravity waves is not included.

The continuity equation of the mass mixing ratio for the major species, N_2, O_2 and O, are solved taking into account the photodissociation of O_2 and oxygen chemistry. The concentrations of CO_2 and NO are prescribed for calculations of the infrared cooling. Schemes for the infrared cooling, absorption of solar extreme ultraviolet (EUV) and ultraviolet (UV) radiations are included in the GCM. The electron density global distribution produced mainly by solar radiation is represented by the Chiu's empirical model (Chiu, 1975). As well as electrons obtained by the Chiu's model, those produced by auroral particles are also taken into account (Fuller-Rowell and Evans, 1987), and the ionospheric conductivity tensor is calculated assuming ion composition at each time step. We also utilize the empirical magnetic convection electric field. Although this GCM does not predict the global distributions of electrons and ions, effects of the ionosphere on the neutral atmosphere, such as the ion drag force, Joule heating and auroral precipitation heating, are taken into account. The molecular diffusions of momentum and heat are also introduced in the upper mesosphere and thermosphere.

Time variations of solar UV and EUV fluxes and geomagnetic activity are frequently observed, and these influence the general circulation in the middle and upper atmosphere. In order to exclude the effects of variations of solar EUV and UV fluxes and geomagnetic activity, the numerical simulation is conducted under solar cycle minimum and geomagnetically quiet conditions. The solar $F_{10.7\mathrm{cm}}$ flux is fixed at 70×10^{-22} W m^{-2} Hz^{-1} during the numerical simulation. The data are sampled at 10-min intervals from 1 June to 14 June. Thus, gravity waves having wave periods longer than 20 min are included in the analyzed data.

3. Results

3.1 Zonal mean field and gravity waves in MF08

The analysis period is identical to that used by MF08, and the distributions of the zonal mean zonal wind and the zonal mean temperature are shown in MF08. The simulated zonal wind and temperature were found to be quite realistic, and our GCM was able to reliably simulate the zonal mean

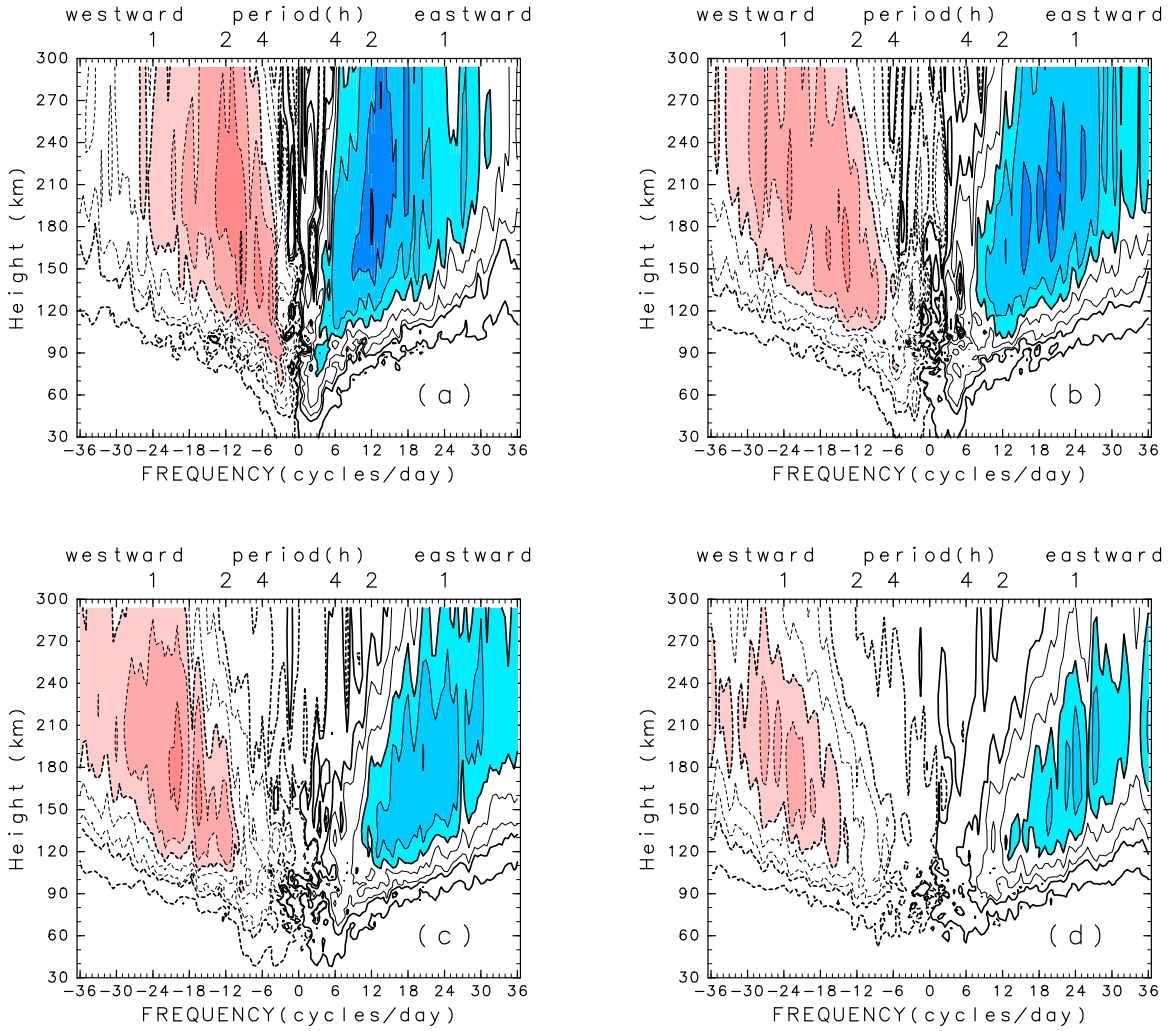

Fig. 1. (a) Frequency-height distribution of the cospectral density of $u'w'$ near the equator (0.4°N) for zonal wave number 20 ($s = 20$, the zonal wavelength $\lambda_x \approx 2000$ km) averaged over the period from 1 June to 14 June. Values of contours are ± 0.01, 0.1, 0.2, 0.5, 1, 2, 5, 10, 20, 50 $\times$ 10^{-2} m^2 s^{-2} day. Solid and broken lines indicate positive and negative values, respectively. Red colors (blue colors) show the region where values are less than -1 (larger than 1). (b) As in Fig. 1(a) except for $s = 40$ ($\lambda_x \approx 1000$ km). (c) As in Fig. 1(a) except for $s = 60$ ($\lambda_x \approx 650$ km). (d) As in Fig. 1(a) except for $s = 80$ ($\lambda_x \approx 500$ km).

field.

MF08 compared the simulated gravity waves in the stratosphere and mesosphere with the observations and showed that the magnitude of the vertical flux of zonal momentum due to gravity waves in the mesopause was similar to that obtained by the radar observations. The effect of gravity wave drag on the zonal mean zonal wind (the EP flux divergence) was also estimated in figure 2 of MF08. It was found that the contribution of the zonal wind acceleration associated with gravity waves to the zonal mean momentum balance was significant not only in the mesosphere but also in the lower thermosphere.

3.2 Gravity waves in the thermosphere

A space-time Fourrier analysis by Hayashi (1971) was performed to investigate the frequency and zonal wave number distribution of gravity waves. Figure 1(a) presents the frequency-height distribution of the cospectral density of $u'w'$ near the equator (0.4°N) for zonal wave number 20 ($s = 20$, the zonal wavelength $\lambda_x \approx 2000$ km) averaged over the period from 1 June to 14 June. Positive (negative) $u'w'$ is dominant for eastward (westward) moving components, indicating an upward energy propagation of gravity waves. The dominant periods of gravity waves at heights of 60, 100 and 150 km are 8, 6 and 3 h, respectively, and gravity waves with periods of about 2 h are dominant above a height of 180 km height. Thus, the dominant periods of gravity waves decrease with height. For the $s = 20$ components, the zonal phase velocities of gravity waves with periods of 6, 3 and 2 h are 93, 185 and 278 m s^{-1}, respectively. This means that gravity waves with a zonal phase velocity of about 100 m s^{-1} dissipate around a height of 120 km, while gravity waves with a zonal phase velocity larger than 200 m s^{-1} can penetrate into the zone at a height of 200 km.

Figure 1(b–d) illustrates the frequency-height distributions of the cospectral density of $u'w'$ for $s = 40$ ($\lambda_x \approx$ 1000 km), 60 ($\lambda_x \approx 650$ km) and 80 ($\lambda_x \approx 500$ km), respectively. The features of distributions of the cospectral density for $s = 40$, 60 and 80 are quite similar to those for $s = 20$. For example, the dominant period of gravity waves with $s = 40$ (80) at a height of 100 km is 3 h (1.5–2 h), while that at a height of 150 km is 1–2 h (1 h). Vadas (2007) investigated the dissipative filtering of grav-

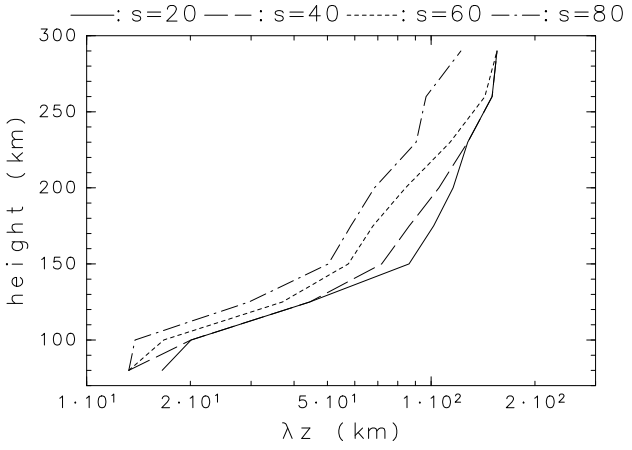

Fig. 2. Height distributions of the vertical wavelength of dominant gravity waves with $s = 20$, 40, 60 and 80. Solid, broken, dotted and chain lines indicates the vertical wavelength with $s = 20$, 40, 60 and 80, respectively. Units are in kilometers.

ity waves in the thermosphere from molecular viscosity and thermal diffusivity and showed dissipation altitudes of gravity waves with 10- to 1200-km horizontal wavelengths in the thermosphere. Figures 4 and 5 of Vadas (2007) clearly show that gravity waves with a zonal phase velocity smaller than 100 m s^{-1} dissipate around heights of 125 km, while gravity waves with larger zonal phase velocity can penetrate into the upper thermosphere. This result is consistent with the results of our present investigation.

Figure 2 shows the height distributions of the dominant vertical wavelength of gravity wave with $s = 20$, 40, 60 and 80, respectively. The dominant vertical wavelength (λ_z) is 15–35 km at a height of 100–120 km and 50–80 km at a height of 150 km. The dominant λ_z is about 100 km around a height of 200 km. Thus, the dominant λ_z increases exponentially with height. For the individual heights, the corresponding dominant λ_z decreases (increases) with the horizontal wave number (the horizontal wavelength). For example, the dominant λ_z at a height of 150 km is 80, 60 and 50 km for $s = 20$ ($\lambda_x \approx 2000$ km), $s = 60$ ($\lambda_x \approx 650$ km) and $s = 80$ ($\lambda_x \approx 500$ km), respectively. Using radar observation, Djuth *et al*. (2004) and Oliver *et al*. (1997) estimated the dominant vertical wavelength of gravity waves. Figure 10 of Oliver *et al*. (1997) shows an exponential increase in λ_z with increasing height. Our results are in good agreement with this observation, although Oliver *et al*. (1997) did not estimate the horizontal wavelength of the gravity wave.

Vadas and Fritts (2005) derived the exact gravity wave anelastic dispersion relation in the presence of the most important forms of dissipation in the thermosphere for high-frequency gravity waves, molecular dissipation and thermal conductivity. They also showed that those gravity waves with a larger vertical wavelength and frequency dissipated at higher altitudes in the thermosphere because they were not as readily dissipated (partially because of their larger vertical group velocity) as those gravity waves with a smaller vertical wavelength and frequency. Vadas and Fritts (2006) and Vadas (2007) investigated the vertical propagation of gravity waves into the thermosphere using the ray tracing method. They showed that the short-period, long-vertical wavelength portions of gravity waves generated by convection could propagate into the thermosphere and that there was an exponential increase in λ_z with height.

3.3 Longitudinal distribution of gravity wave activity

The longitudinal distribution of gravity wave activity in the equatorial thermosphere and upward propagation of gravity waves from the lower atmosphere to the upper thermosphere were also investigated. The short-period gravity waves are dominant in the thermosphere, so that the wind and temperature components with a period varying from 1 to 4 h can be extracted using a band-pass filter. Figure 3(a) presents the longitudinal distribution of the total (kinetic plus potential) energy associated with the short-period gravity waves near the equator (averaged over 10°N to 10°S) at a height of 300 km during the period from 1 June to 14 June. The significant maximum of the total energy is located around 150–180°E, and there is a faint enhancement of the energy around 10–40°E. The positions and shapes of the peaks at a height of 200 km (Fig. 3(b)) are quite similar to those at 300 km. The longitudinal distribution of the total energy near the equator at a height of 100 km is shown in Fig. 3(c). The peaks of the energy associated with the short-period gravity waves around 150–180°E and 10–40°E are found in the height range from 100 to 300 km. In contrast, the peak of the total energy around 250–280°E appears at a height of 100 km, but this peak becomes unclear in the 200- to 300-km height region.

Figure 3(d) shows the longitude-height section of the total energy for the short-period gravity waves near the equator. There are three maxima of gravity wave energy in the mesosphere: 10–30°E, 120–150°E and 260–290°E. The energy peak around 120–150°E is two- to threefold larger than those at 10–30°E and 260–290°E. The maximum around 120–150°E moves eastward with increasing height, while the maxima around 10–30°E and 260–290°E moves slightly westward with increasing height. However, the longitudinal variation in the energy due to the short-period gravity waves in the stratosphere and mesosphere are similar to that in the thermosphere. Figure 3(e) presents the longitudinal distribution of the rainfall rate averaged over 10°N to 10°S. The longitudinal distribution of the energy due to the short-period gravity waves in the stratosphere and mesosphere is closely related with the longitudinal location of the large rainfall rate near the equator. This correlation is explained by the fact that the gravity wave is mainly generated by cumulus convection.

In order to examine the vertical propagation of the short-period gravity waves, we calculated the vertical energy flux ($\rho\phi' w'$) (ρ and ϕ' are the atmospheric density and the geopotential height fluctuation component, respectively) associated with the short-period gravity waves. Figure 4 illustrates the longitudinal distribution of $\rho\phi' w'$ near the equator. A positive (negative) $\rho\phi' w'$ value indicates upward (downward) energy propagation. Positive values are found for all the regions from the troposphere to the upper thermosphere, indicating that upward energy propagation due to the short-period gravity waves is a dominant force. Upward energy propagation above a height of 100 km is enhanced around 150–180°E where the total energy due to the short-period gravity waves is also at a maximum. This enhance-

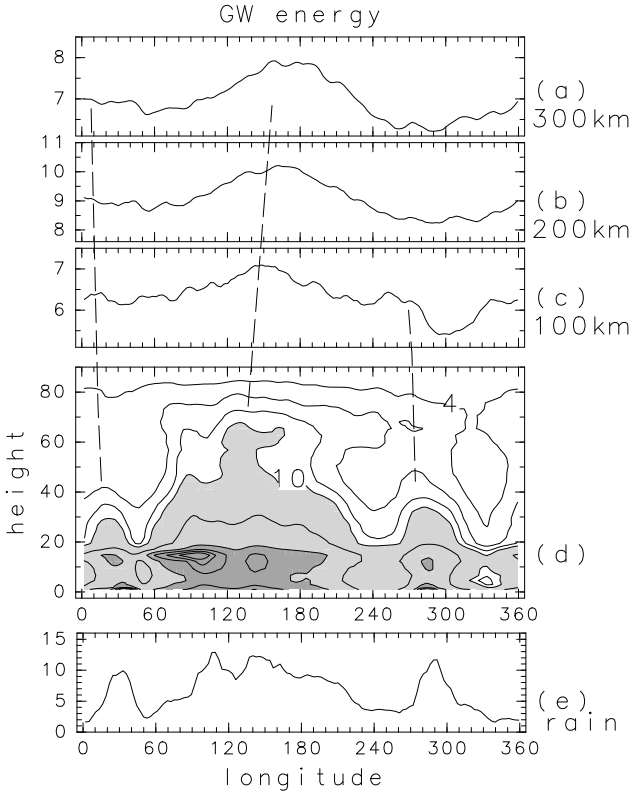

Fig. 3. (a) Longitudinal distribution of the total (kinetic plus potential) energy associated with the short-period gravity waves near the equator (averaged over 10°N to 10°S) at a height of 300 km during the period from 1 June to 14 June; units are $\times 10^{-8}$ kg m^2 s^{-2}. (b) As in Fig. 3(a) except for a height of 200 km; units are $\times 10^{-7}$ kg m^2 s^{-2}. (c) As in Fig. 3(a) except for a height of 100 km; units are $\times 10^{-4}$ kg m^2 s^{-2}. (d) Longitude-height section of the total (kinetic plus potential) energy associated with the short-period gravity waves near the equator (averaged over 10°N to 10°S); values of contours are 4, 6, 8, 10, 20, 40, 60, 80, 100×10^{-3} kg m^2 s^{-2}. Lightly (darkly) shades are the regions where the energy $>10 \times 10^{-3}$ (40×10^{-3}). (e) Longitudinal distribution of the rainfall rate near the equator (averaged over 10°N to 10°S) during the period from 1 June to 14 June; units are millimeters per day.

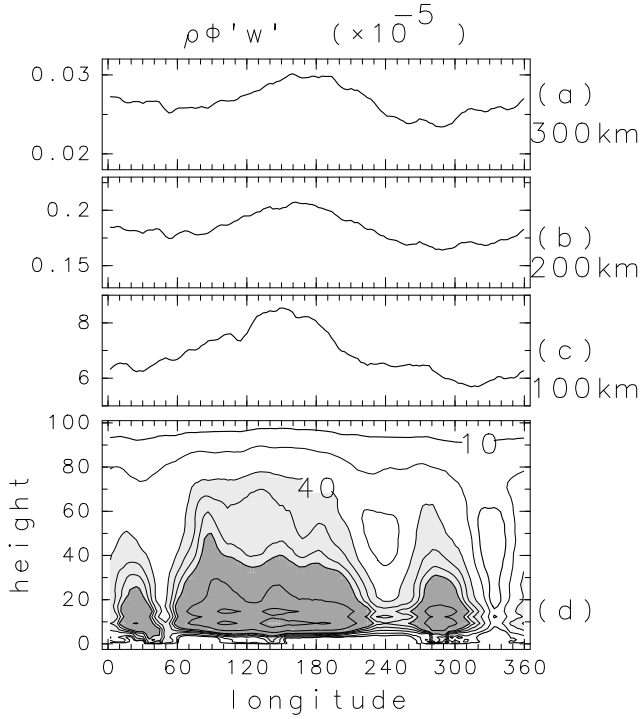

Fig. 4. (a) Longitudinal distribution of vertical flux of energy for the short-period gravity waves (1–4 h) averaged over 14 days at a height of 300 km (1–14 June); units are $\times 10^{-5}$ kg m^{-1} s^{-1}. (b) As in Fig. 4(a), except for a height of 200 km. (c) As in Fig. 4(a), except for a height of 100 km. (d) Longitude-height section of vertical flux of energy for the short-period gravity waves (1–4 h); values of contours are 10, 20, 40, 60, 80, 100, 200, 400 $\times 10^{-5}$ kg m^{-1} s^{-1}. Lightly (darkly) shades are the regions where $\rho\phi' w' > 40 \times 10^{-5}$ (100×10^{-5}).

ment of upward energy flux around 150°E is also found in the stratosphere and mesosphere. Upward energy flux due to the short-period gravity waves in the stratosphere and mesosphere is significant over those regions where the cumulus convection is enhanced (10–30°E, 90–180°E and 260–290°E). As mentioned above, the dominant vertical wavelength of the short-period gravity waves is 50 km at a height of 150 km and exceeds 100 km above a height of 200 km, indicating that the vertical group velocity associated with the short-period gravity waves is very large. Thus, our results indicate that the strong energy flux due to gravity waves from the enhanced cumulus convective activity can penetrate into the upper thermosphere.

Using GPS/MET radio occultation, Hocke and Tsuda (2001) and Tsuda and Hocke (2004) investigated the longitudinal distribution of plasma irregularity in the MLT region (the E-region) and stratospheric gravity wave activity at low latitudes. These researchers found that the maxima of enhanced stratospheric gravity waves activity and plasma irregularity in the MLT region were located over the region where cumulus convective activity was enhanced. This result is consistent with our result. However, our results show that the longitudinal variation of the gravity wave energy in the upper thermosphere is also closely related to that of the convective activity and the stratospheric gravity wave activity.

4. Discussion

4.1 Seasonal variations in gravity wave activity in the thermosphere

We have shown that the short-period gravity waves were dominant in the thermosphere and that upward propagation from the lower atmosphere occurred. In particular, the longitudinal variation in the gravity wave energy in the equatorial thermosphere was correlated with that of the stratospheric gravity wave energy and the convective activity in the tropical troposphere. The analysis carried out in the previous section was conducted during the period from 1 June to 14 June. To be able to determine seasonal variation in gravity wave activity in the equatorial thermosphere, we also performed a preliminary analysis during the period from 21 March to 31 March.

Figure 5 illustrates the longitudinal distribution of the total (kinetic pus potential) energy associated with the short-period gravity waves near the equator (averaged over 10°N to 10°S) during the period from 21 March to 31 March. The energy at heights of 200 and 300 km has maxima around 0°E, 120–130°E, 200–210°E and 290–300°E, with a weak peak appearing around 70–80°E. These energy peaks in the thermosphere are correlated with the energy peaks at

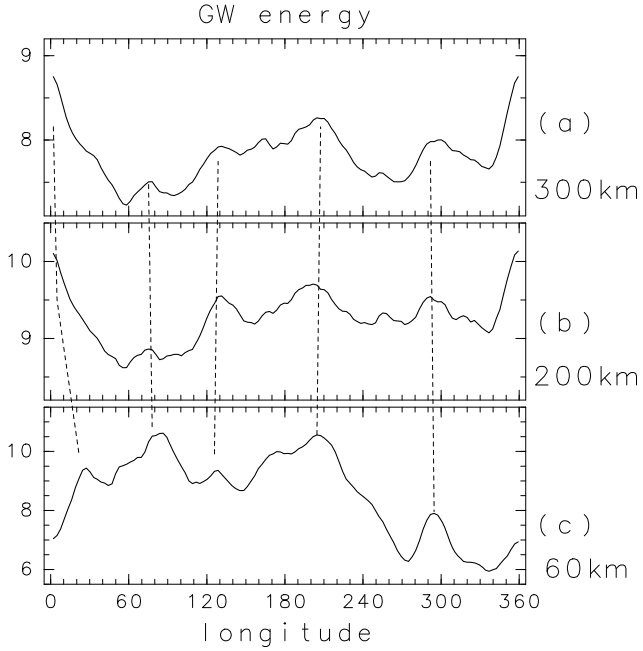

Fig. 5. (a) Longitudinal distribution of the total (kinetic pus potential) energy associated with the short-period gravity waves near the equator (10°N–10°S) at a height of 300 km averaged over the period from 21 March to 31 March; units are $\times 10^{-8}$ kg m^2 s^{-2}. (b) As in Fig. 5(a) except for a height of 200 km; units are $\times 10^{-7}$ kg m^2 s^{-2}. (c) As in Fig. 5(a) except for a height of 60 km; units are $\times 10^{-3}$ kg m^2 s^{-2}.

a height of 60 km except for the region around 0–30°E. The energy peak around 0°E does not appear at a height of 60 km. Another peak is located at 20–30°E at a height of 60 km, and this peak moves westward with height, corresponding to the peak around 0°E at heights of 200 and 300 km. The longitudinal variation in the total energy below a height of 60 km is similar to that at a height of 60 km (not shown). Thus, the longitudinal variation in gravity wave activity in the thermosphere is affected by the variation in gravity wave activity in the lower atmosphere. The shapes and peaks of the gravity wave energy distribution in March are quite different from those in June. The longitudinal distribution of the moist convection center in the tropical troposphere also varies with season. These results indicate that seasonal variation of gravity wave activity in the equatorial thermosphere is influenced by seasonal variation of the gravity wave energy distribution in the lower atmosphere that is generated by seasonal variation of the longitudinal distribution of the moist convection activity in the tropical troposphere. We performed the analysis in June and March, but the analysis period (the 14-day dataset in June and the 10-day dataset in March) is too short to examine seasonal variations in gravity wave activity in the equatorial thermosphere. A 1-year dataset is desirable to study seasonal variation.

In GCMs, moist convection is not resolved explicitly because of its sparse horizontal resolution. In our study, Kuo's cumulus parameterization was used; however, in other GCMs, various types of cumulus parameterizations, such as moist convective adjustment and Arakawa-Schubert's scheme, were used. Horinouchi *et al.* (2003) investigated the effects of cumulus parameterization on the variability of rainfall rate and simulated waves in the equatorial middle atmosphere. They showed that the choice of cumulus parameterization had an impact on the vertically propagating waves in the equatorial middle atmosphere. Thus, a series of GCM experiments with other cumulus parameterizations may be necessary.

4.2 Relation with ionospheric variability

In this subsection, we discuss fluctuations of the horizontal wind due to gravity waves and their relations with ionospheric variability. One of the more significant phenomena in the equatorial ionosphere is the presence of plasma bubbles. Plasma bubbles are generated in the bottomside of the F-region after sunset through the Rayleigh-Taylor instability. One of the candidates for triggering the Rayleigh-Taylor instability is gravity waves in the equatorial thermosphere (e.g., Kelly *et al.*, 1981; Lin *et al.*, 2005). Gravity waves can produce a sinusoidal oscillation of the altitude of the bottomside of the F-region (Singh *et al.*, 1997). Ogawa *et al.* (2005) found wavy plasma structures (a few hundreds to 1000 km across) within the northern and southern equatorial anomaly crest. Gravity waves are considered to play an important role in the seeding process of plasma bubbles.

To demonstrate the zonal wind fluctuation due to the short-period gravity waves, in Fig. 6 we show longitude (0–45°E)-time sections of the zonal wind fluctuation with a period of 1–4 h near the equator (0.4°N) during 3 days (June 2–4) at a height of 250 km. The diurnal variation in the zonal wind at 0.4°N and 0°E averaged over the period from 1 June to 14 June is also illustrated in the right panel of Fig. 6. Wavy structures with the zonal scale of a several hundred kilometers to 1000 are clearly seen. Fluctuations with periods of 1–2 h are significant, and the amplitudes sometimes exceed 50 m s^{-1}. Westward moving waves are dominant during the night time when the background zonal wind is eastward, although eastward moving waves are sometimes found after sunset. The amplitude of the fluctuations of the zonal wind has day-to-day variations. Namely, wave activity after sunset is stronger in 4 June than in 2 June. These results suggest that the short-period gravity waves in the neutral atmosphere induce the wavy plasma structures and may induce the Rayleigh-Taylor instability. In the GCM used in the present study, however, the global distributions of electrons and ions are prescribed by using an empirical model—and are therefore not predicted. As the electrons and ions are affected by the neutral gas motion, we suggest that fluctuations associated with gravity waves influence the seeding process of plasma bubbles. In order to investigate the effects of gravity waves on the ionospheric variability in detail, a GCM that solves the momentum and energy equations of electrons and ions needs to be developed. A new GCM will be able to predict the fluctuations of the ionosphere induced by the variations in the neutral atmosphere.

As mentioned above, the gravity wave activity in the equatorial thermosphere has significant longitudinal variation. The amplitude of the wind fluctuation due to the short-period gravity waves is larger at 150–180°E than at the other regions. This result suggests that wavy plasma structures in the bottomside of the F-region can be formed more frequently around 150–180°E due to the stronger gravity wave

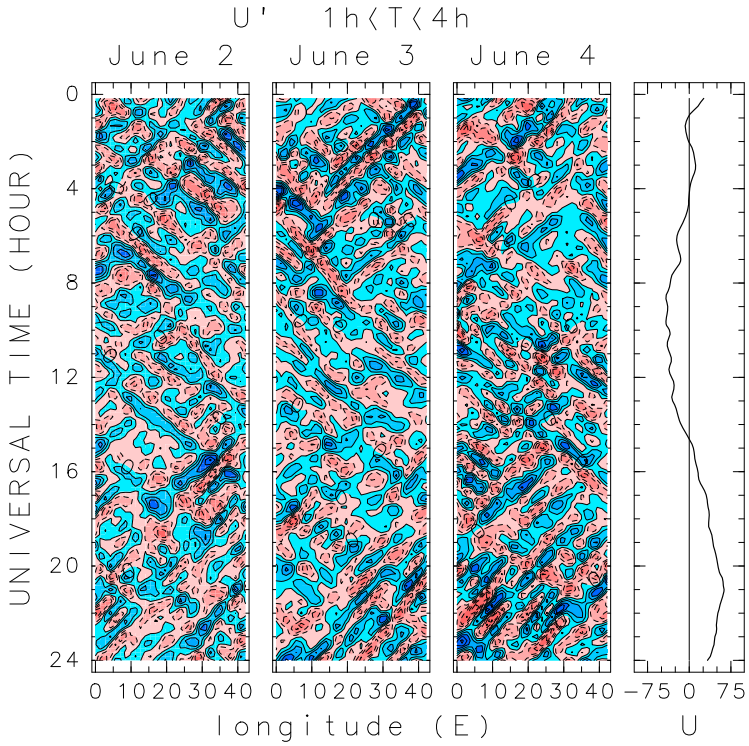

Fig. 6. Longitude (0–45°E)-time sections of the zonal wind fluctuation with a period from 1 to 4 h near the equator (0.4°N) during 3 days (June 2–4) at a height of 250 km. Contour intervals are 25 m s^{-1}. Negative values (dotted lines) indicate a westward wind. Red (blue) colors show westward (eastward) wind components. The right panel shows the diurnal variation of the zonal wind at 0.4°N and 0°E averaged over the period from 1 June to 14 June.

activity. We suggest that the longitudinal variation of the gravity wave activity in the thermosphere induces the longitudinal variation of the ionosphere.

5. Summary

Using a GCM that contains the region from the ground surface to the upper thermosphere, we have examined the behavior of gravity waves in the thermosphere. The horizontal resolution in the GCM was roughly equivalent to a grid spacing of 140 km. At a height of 100 km, the dominant periods of gravity waves for zonal wave number 20 ($\lambda_x \approx 2000$ km), 40 ($\lambda_x \approx 1000$ km) and 80 ($\lambda_x \approx 500$ km) are 6, 3 and 1.5–2 h, respectively. The dominant period (zonal phase velocity) of gravity waves decreases (increases) with height. Gravity waves with a zonal phase velocity of 100 m s^{-1} dissipate around a height of 120 km, while gravity waves with a zonal phase velocity larger than 200 m s^{-1} can penetrate to a height of 200 km. The dominant λ_z is 15–35 km, 50–80 km and about 100 km at heights of 100–120, 150 and 200 km, respectively. The dominant λ_z increases exponentially with height.

We examined the longitudinal distribution of gravity wave activity in the equatorial thermosphere and the upward propagation of gravity waves from the lower atmosphere. The longitudinal variation of gravity wave activity in the equatorial thermosphere is quite similar to that of the gravity wave activity in the stratosphere and mesosphere and the convective activity in the tropical troposphere. Upward energy flux due to the short-period gravity waves in the stratosphere and mesosphere is significant over the regions where the cumulus convection is enhanced. Our results indicate that the strong energy flux due to gravity waves from the enhanced cumulus convective activity can penetrate into the upper thermosphere.

We have also discussed fluctuations of the horizontal wind associated with gravity waves and its relation to the ionospheric variation. The short-period gravity waves that are generated in the lower atmosphere and propagate into the thermosphere induce wavy structures of the zonal wind in the upper thermosphere. Fluctuations due to the short-period gravity waves with periods of 1–2 h are significant, and its amplitudes sometimes exceed 50 m s^{-1}. These results suggest that gravity waves in the neutral atmosphere can produce the wavy plasma structures and may induce plasma bubbles. However, in the GCM used in our investigation, the global distributions of electrons and ions are prescribed using an empirical model—and are not predicted. In order to investigate the effects of gravity waves on the ionospheric variability in detail, it will be necessary to develop a GCM that solves the momentum and energy equations of electrons and ions. A new GCM will be able to predict the fluctuations of the ionosphere induced by the neutral atmospheric variation.

Acknowledgments. We are grateful to the reviewers for their helpful comments on the original manuscript. This work was supported in part by a Grant-in-aid for Scientific Research by the Ministry of Education, Culture, Sports, Science and Technology, Japan, and the joint research program of the Solar-Terrestrial Environment Laboratory, Nagoya University. The computations in this study were partially performed on a Fujitsu HPC2500 at the Information Technology Center, Nagoya University. The GFD/DENNOU Library was used for drawing figures.

References

Chiu, Y. T., An improved phenomenological model of ionospheric density, *J. Atmos. Terr. Phys.*, **37**, 1563–1570, 1975.

Djuth, F. T., M. P. Sulzer, S. A. Gonzales, J. D. Mathews, J. H. Elder, and R. L. Walterscheid, A continuum of gravity waves in the Arecibo thermosphere?, *Geophys. Res. Lett.*, **31**, L16801, doi:10.1029/2003GL019376, 2004.

Fuller-Rowell, T. J. and D. S. Evans, Height-integrated Pedersen and Hall conductivity patterns inferred from the TIROS-NOAA satellite data, *J. Geophys. Res.*, **92**, 7606–7618, 1987.

Hayashi, Y., A generalized method of resolving disturbances into progressive and retrogressive waves by space Fourier and time cross-spectral analyses, *J. Meteor. Soc. Jpn.*, **49**, 125–128, 1971.

Hayashi, Y., D. G. Golder, J. D. Mahlman, and S. Miyahara, The effect of horizontal resolution on gravity waves simulated by the GFDL SKYHI general circulation model, *PAGEOPH*, **130**, 421–443, 1989.

Hayashi, Y., D. G. Gloder, and P. W. Jones, Tropical gravity waves and super clusters simulated by high-horizontal resolution SKYHI general circulation model, *J. Meteor. Soc. Jpn.*, **75**, 1125–1139, 1997.

Hocke, K. and K. Schlegel, A review of atmospheric gravity waves and traveling ionospheric disturbances:1982–1995, *Ann. Geophys.*, **14**, 917–940, 1996.

Hocke, K. and T. Tsuda, Gravity waves and ionospheric irregularities over tropical convection zones observed by GPS/MET radio occultation, *Geophys. Res. Lett.*, **28**, 2815–2818, 2001.

Horinouchi, T., T. Nakamura, and J. Kosaka, Convectively generated mesoscale gravity waves simulated throughout the middle atmosphere, *Geophys. Res. Lett.*, **29**(21), 2007, doi:10.1029/2002GL016069, 2002.

Horinouchi, T., S. Pawson, K. Shibata, U. Langematz, E. Manzin, M. A. Giorgetta, F. Sassi, R. J. Wilson, K. Hamilton, J. Grandpre, and A. A. Scaife, Tropical cumulus convection and upward-propagating waves in middle-atmosphere GCMs, *J. Atmos. Sci.*, **60**, 2765–2782, 2003.

Jones, P. W., K. Hamilton, and R. J. Wilson, A very high resolution general circulation model simulation of the global circulation in austral winter, *J. Atmos. Sci.*, **54**, 1107–1116, 1997.

Kelly, M. C., M. F. Larsen, C. M. Swenson, and T. F. Wheeler, Gravity wave initiation of equatorial spread F: A case study, *J. Geophys. Res.*, **86**, 9087–9100, 1981.

Lin, C. S., T. J. Immel, H. C. Yeh, S. B. Mende, and J. L. Burch, Simultaneous observations of equatorial plasma depletion by IMAGE and ROCSAT-1 satellites, *J. Geophys. Res.*, **110**, A06304, doi:10.1029/2004JA010774, 2005.

Lindzen, R. S., Turbulence and stress owing to gravity wave and tidal breakdown, *J. Geophys. Res.*, **86**, 9707–9714, 1981.

Matsuno, T., A quasi one-dimensional model of the middle atmosphere circulation interacting with internal gravity waves, *J. Meteor. Soc. Jpn.*, **60**, 215–226, 1982.

McFarlane, N. A., The effect of orographically excited gravity wave drag on the general circulation of the lower stratosphere and troposphere, *J. Atmos. Sci.*, **44**, 1775–1800, 1987.

Miyahara, S., Y. Yoshida, and Y. Miyoshi, Dynamic coupling between the lower and upper atmosphere by tides and gravity waves, *J. Atmos. Terr. Phys.*, **55**, 1039–1053, 1993.

Miyoshi, Y., Numerical simulation of the 5-day and 16-day waves in the mesopause region, *Earth Planets Space*, **51**, 763–772, 1999.

Miyoshi, Y., Temporal variation of nonmigrating diurnal tide and its relation with the moist convective activity, *Geophys. Res. Lett.*, **33**, L11815, doi:10.1029/2006GL026072, 2006.

Miyoshi, Y. and H. Fujiwara, Day-to-day variations of migrating diurnal tide simulated by a GCM from the ground surface to the exobase, *Geophys. Res. Lett.*, **30**, 1789, doi:10.1029/2003GL017695, 2003.

Miyoshi, Y. and H. Fujiwara, Excitation mechanism of intraseasonal oscillation in the equatorial mesosphere and lower thermosphere, *J. Geophys. Res.*, **111**, D14108, doi:10.1029/2005JD006993, 2006.

Miyoshi, Y. and H. Fujiwara, Gravity waves in the thermosphere simulated by a general circulation model, *J. Geophys. Res.*, **113**, D01101, doi:10.1029/2007JD008874, 2008.

Ogawa, T., E. Sagawa, Y. Otsuka, K. Shiokawa, T. J. Immel, S. B. Mende, and P. Wilkinson, Simultaneous ground- and satellite-based airglow observations of geomagnetic conjugate plasma bubbles in the equatorial anomaly, *Earth Planets Space*, **57**, 385–392, 2005.

Oliver, W. L., Y. Otsuka, M. Sato, T. Takami, and S. Fukao, A climatology of F region gravity waves propagation over the middle and upper atmosphere radar, *J. Geophys. Res.*, **102**, 14499–14512, 1997.

Reid, I. M. and R. A. Vincent, Measurements of mesospheric gravity wave momentum fluxes and mean flow accelerations at Adelaide, Australia, *J. Atmos. Terr. Phys.*, **49**, 443–460, 1987.

Sato, K., T. Kumakura, and M. Takahashi, Gravity waves appearing in a high-resolution GCM simulation, *J. Atmos. Sci.*, **56**, 1005–1018, 1999.

Singh, S., F. S. Johnson, and R. A. Power, Gravity wave seeding of equatorial plasama bubbles, *J. Geophys. Res.*, **102**, 7399–7410, 1997.

Tsuda, T. and K. Hocke, Application of GPS radio occultation data for studies of atmospheric waves in the middle atmosphere and ionosphere, *J. Meteor. Soc. Jpn.*, **82**, 419–426, 2004.

Tsuda, T., Y. Murayama, M. Yamamoto, S. Kato, and S. Fukao, Seasonal variation of momentum flux in the mesosphere observed with the MU radar, *Geophys. Res. Lett.*, **17**, 725–728, 1990.

Vadas, S. L., Horizontal and vertical propagation and dissipation of gravity waves in the thermosphere from lower atmospheric and thermospheric sources, *J. Geophys. Res.*, **112**, A06305, doi:10.1029/20056JA011845, 2007.

Vadas, S. L. and D. C. Fritts, Thermospheric responses to gravity waves arising from mesoscale convective complexes, *J. Atmos. Sol.-Terr. Phys.*, **66**, 781–804, 2004.

Vadas, S. L. and D. C. Fritts, Thermospheric responses to gravity waves: Influences of increasing viscosity and thermal diffusivity, *J. Geophys. Res.*, **110**, D15103, doi:10.1029/2004JD005574, 2005.

Vadas, S. L. and D. C. Fritts, Influences of solar variability on gravity wave structure and dissipation in the thermosphere from tropospheric convection, *J. Geophys. Res.*, **111**, A10S12, doi:10.1029/2005JA011510, 2006.

Vincent, R. A. and D. C. Fritts, A climatology of gravity wave motions in the mesopause region at Adelaide, Australia, *J. Atmos. Sci.*, **44**, 748–760, 1987.

Waldock, P. J. and T. B. Jones, Source regions of medium-scale traveling disturbances observed at mid-latitudes, *J. Atmos. Terr. Phys.*, **49**, 105–114, 1987.

Y. Miyoshi (e-mail: miyoshi@geo.kyushu-u.ac.jp) and H. Fujiwara